Author Manuscript

Author Manuscript

Author Manuscript

Author Manuscript

HHS Public Access

Author manuscript

Heart Rhythm. Author manuscript; available in PMC 2024 January 01.

Published in final edited form as:

Heart Rhythm. 2023 January ; 20(1): 122–133. doi:10.1016/j.hrthm.2022.08.039.

Three-Dimensional Functional Anatomy of Human Sinoatrial node for Epicardial and Endocardial Mapping and Ablation

Anuradha Kalyanasundaram, PhD[1,3], **Ning Li, MD, PhD**[1,3], **Ralph S. Augostini, MD**[2,3], **Raul Weiss, MD**[2,3], **John D. Hummel, MD**[2,3], **Vadim V. Fedorov, PhD**[1,3]

[1]-Department of Physiology & Cell Biology, The Ohio State University Wexner Medical Center, Columbus, OH

[2]-Division of Cardiovascular Medicine, The Ohio State University Wexner Medical Center, Columbus, OH

[3]-Bob and Corrine Frick Center for Heart Failure and Arrhythmia, The Ohio State University Wexner Medical Center, Columbus, OH

Abstract

The sinoatrial node (SAN) is the primary pacemaker of the human heart. It is a single, elongated three-dimensional (3D) intramural fibrotic structure located at the junction of the superior vena cava intercaval region bordering the crista terminalis (CT). SAN activation originates in the intranodal pacemakers and is conducted to the atria through one or more discrete sinoatrial conduction pathways. The complexity of the 3D SAN pacemaker structure and intramural conduction are underappreciated during clinical multi-electrode mapping and ablation procedures of SAN and atrial arrhythmias. In fact, defining and targeting SAN is extremely challenging because even during sinus rhythm, surface only multi-electrode mapping may not define the leading pacemaker sites in intramural SAN but instead misinterpret them as epicardial or endocardial exit sites through sinoatrial conduction pathways. These SAN exit sites may be distributed up to 50 mm along the CT beyond the ~20 mm long anatomical SAN structure. Moreover, since SAN reentry tachycardia beats may exit through the same sinoatrial conduction pathway as during sinus rhythm, many SAN arrhythmias are underdiagnosed. Misinterpretation of arrhythmia sources and/or mechanisms (e.g., enhanced automaticity, intranodal vs CT reentry) limit diagnosis and success of catheter ablation treatments for poorly understood SAN arrhythmias. The aim of this review is to provide a state-of-the-art overview of the 3D structure and function of the human SAN complex, mechanisms of SAN arrhythmias and available approaches for electrophysiological mapping, 3D structural imaging, pharmacological interventions and ablation to improve diagnosis and mechanistic treatment of SAN and atrial arrhythmias.

Corresponding author: Vadim V. Fedorov, PhD, The Ohio State University Wexner Medical Center, 5196 Graves Hall, 333 W 10th Ave, Columbus OH 43210-1218, vadim.fedorov@osumc.edu.

Publisher's Disclaimer: This is a PDF file of an article that has undergone enhancements after acceptance, such as the addition of a cover page and metadata, and formatting for readability, but it is not yet the definitive version of record. This version will undergo additional copyediting, typesetting and review before it is published in its final form, but we are providing this version to give early visibility of the article. Please note that, during the production process, errors may be discovered which could affect the content, and all legal disclaimers that apply to the journal pertain.

Disclosures: VVF has been a consultant for Atricure. The remaining authors have nothing to disclose.

Author Manuscript Author Manuscript Author Manuscript Author Manuscript

Graphical Abstract

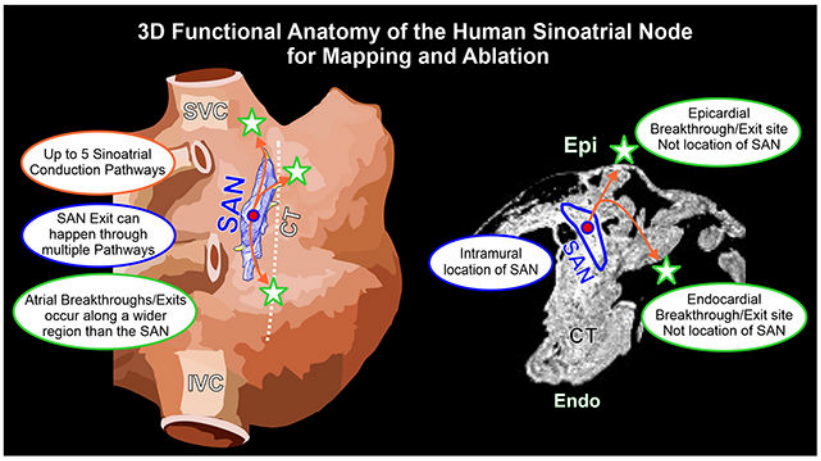

Keywords

sinoatrial node; crista terminalis; 3D electro-anatomical mapping; sinus tachycardia; optical mapping; adenosine; reentry; ablation

INTRODUCTION

The sinoatrial node (SAN) is the primary pacemaker of the human heart. Beginning from the original discovery by Keith and Flack in 1907[1], multiple histological studies have defined the human SAN as a single elongated, fibrotic structure located at the junction of the superior vena cava (SVC)-cranial intercaval region (Figure 1A). Impairments in both activation and conduction result in SAN arrhythmias, including severe bradycardia due to SAN arrest and exit block and/or tachycardia due to SAN reentry (SANRT) or abnormally enhanced SAN pacemaker automaticity[2, 3]. Clinical multi-electrode mapping is unable[4] to assess intramural conduction in the 3D SAN pacemaker complex, which may lead to misinterpretation of arrhythmic sources and/or mechanisms. An improved understanding of the 3D functional anatomy of the human SAN pacemaker-conduction complex may help design efficient mapping and ablation approaches to treat SAN related tachycardia. The goal of this review is to provide a state-of-the-art comprehensive overview of the 3D structure-function of the human SAN, clinical and experimental electrophysiological SAN mapping approaches, 3D structural imaging modalities (magnetic resonance imaging (MRI) and computed tomography) and pharmacological interventions (e.g. adenosine). We will also discuss the unique role of crista terminalis (CT) in SAN arrhythmias, evaluate SAN/CT ablation studies, and provide insights from these existing studies to improve SAN arrhythmia for optimal outcomes.

Author Manuscript Author Manuscript Author Manuscript Author Manuscript

3D STRUCTURE AND FUNCTION OF THE HUMAN SAN PACEMAKER CONDUCTION COMPLEX

The human SAN is a single, elongated 3D intramural fibrotic pacemaker structure, which runs parallel to the CT (Figure 1B). The position of the SAN is intramural in the sense that it is a discrete structure located at a depth of ~1-3mm from the epicardium (Figure 1C), separated from the endocardium and epicardium by layers of fibrosis, fat and atrial myocardium. It is typically tilted such that the SAN head (superior third) lies relatively sub-epicardially and the SAN tail (inferior third) sub-endocardially [2]. The electrical impulse that initiates the normal sinus rhythm originates in the SAN pacemaker cardiomyocytes, which are enmeshed and electrically insulated within strands of dense connective tissue, to create a distinct SAN pacemaker complex[2, 5–7]. In the adult human heart, the size of SAN structure can significantly vary making its exact location difficult to define in patients. Multiple studies have described the 3D structure of the human SAN [5, 7–9], which can be between ~11 to 30mm in length[5, 7, 10], ~2-6mm width and a thickness of ~2.2-2.6mm (Figure 1D).

Since the normal adult SAN structure consists of ~40-55% dense fibrotic tissue[11], cardiac fibrosis imaging techniques including high-resolution delay-enhanced MRI, allow identification of the human 3D SAN structure both in-vivo and ex-vivo[12]. The SAN artery runs through the center of the human SAN (Figure 1C–E) and is often considered a prominent landmark to identify the SAN[13]. Fibrosis, fatty tissue and/or discontinuous myofibers along the SAN border electrically insulate the SAN pacemaker cells from the hyperpolarizing effects of the surrounding myocardium, efficiently protecting normal automaticity[5] (Figure 1E). The human SAN pacemaker cells lack high conductance gap junction proteins Connexin 43 (Cx43)[5, 14], have low expression of cardiac Nav1.5 sodium channels [3, 14] but higher neuronal Nav1.6 sodium channels and highest cardiac expression of pacemaker “funny” channels HCN1 and HCN4[14], which explains slower but robust intranodal conduction (1-16 cm/sec) and fastest automaticity in the SAN center pacemaker. HCN1/4[14] and adenosine receptor 1 (AR1), GIRK1/4[2] potassium channels expressions are usually higher in SAN center than tail/head but with heart-specific variations.

PREFERENTIAL SINOATRIAL CONDUCTION PATHWAYS

Pioneering atrial epicardial multi-electrode mapping studies in canine[15] and human[16] hearts by the Schuessler and Boineau group led to the suggestion of a widely distributed “atrial pacemaker complex” and existence of specific exit sites for SAN impulses. Later, Bromberg et al’s[17] elegant ex-vivo canine study showed that leading SAN pacemaker activation can precede the earliest atrial surface activation site (EAS) by > 100ms and located > 10mm from each other[17] (Figure 2A). Unlike clinical surface electrode studies, which cannot define intramural activation within the SAN complex, sub-surface near-infrared optical mapping (NIOM) reliably delineates activation and conduction within the human SAN and preferential sinoatrial conduction pathways (SACPs)[2, 3](Figure 2 B–C). Novel near-infrared voltage-sensitive dyes (e.g. di-4-ANBDQBS) can resolve intramural cardiac conduction up to 4mm[18, 19] or even up to 8-10mm with transillumination and dual-sided

Author Manuscript Author Manuscript Author Manuscript Author Manuscript

endo-epicardial NIOM mapping, thereby unmasking intramural activation of the SAN[20]. Analytical approaches allow the separation[21] and/or the extraction[5] of intramural SAN conduction from atrial activation (Figure 2D).

The 2017 Li et al's[2] integrated NIOM-3D structural study showed that the human SAN is functionally insulated/discontinued from the atria by fibrosis, fat and myofiber discontinuity except for the 2-5 discrete SACPs. They were categorized based on their general anatomic locations as lateral superior/middle/inferior, SVC, and septal pathways[2, 3] (Figures 2B). NIOM successfully identified preferential SACPs in thirty-two human SANs (19-69 y.o.) collectively mapped in five published ex-vivo human studies[2, 3, 5, 12, 22]. Human SACPs are composed of several discrete branching myofiber tracts, ~280μm thick and ~2-3mm long, characterized by myofibers of pacemaker cells transitioning to atrial cardiomyocytes, which form continuous, uninterrupted electrical coupling between the SAN pacemaker cells and atrial myocardium[5] (Figure 3A). Csepe et al[5] revealed a smooth transition in increasing cell diameter from SAN to atrial regions only in SACP regions and Cx43-negative SAN pacemaker cells progressively transition to distinct Cx43 gap junctions in the atria (Figure 3B) suggesting that SACP cells may show a morphological and molecular phenotype intermediate between SAN and atria. Importantly, these SACPs between the SAN and atrial myocardium are not the "specialized atrial conducting pathways" suggested to exist between the SAN and atrioventricular node within atrial walls but never proven due to lack of any morphological evidence, as recently reviewed by Anderson et al[23].

Although 3D histology-based SAN models[9, 24, 25] have been developed from 1960s[6, 25], none showed distinct SACPs. Later in 2010, developments in intramural optical mapping allowed Fedorov et al[18] to identify and demonstrate the presence of distinct SACPs in the human SAN. Subsequently, Chandler et al in 2011[9] provided a 3D human SAN anatomical model, which included myocyte orientation based on 400μm DT-MRI as well as description of a novel "paranodal area….running alongside the sinus node" that did not show discernible expression of HCN4. Although the area was suggested to have a role in pacemaking and widespread distribution of the leading pacemaker site in human atria, no direct electrophysiological recordings were reported by the authors or any other study to demonstrate its function. Furthermore, the Chandler et al's anatomical 3D model[9] did not include SACP. The differences were previously discussed in detail in Csepe et al[5] where high-resolution NIOM (330x330μm^2) was integrated with 3D structural approaches[2, 3], including serial histological sections parallel to epicardium (0.5x0.5μm^2 X-Y resolution, 13-21μm epicardium to endocardium section steps). 3D fiber orientation analysis with fiber tracking[5] allowed for revealing the continuous SACP myofiber tracts connecting the SAN to the atria, which transmit electrical impulses to the atrial myocardium and correspond to the discrete EASs seen during SR. Importantly, other SAN models including Chandler et al[9] had large steps between subsequent histological slides and did not include direct functional validation of SAN conduction and 3D myofiber tracking, which may explain the absence 3D SACP structures in these models. Otherwise, all of these 3D models described similar 3D dimensions and the shape of SAN. Recently, the presence of the SACP's has been corroborated by Yamabe et al[26] by targeting SACPs for ablation of SANRT.

Author Manuscript Author Manuscript Author Manuscript Author Manuscript

DISCRETE SUPERIOR-INFERIOR SAN EXIT PATTERNS ALONG CT DURING SINUS RHYTHM

Ex-vivo human SAN NIOM studies[2] have shown that during normal sinus rhythm, excitation originates in one of the intranodal pacemaker compartments, and then is preferentially delivered (exited) to the atria via either one or two lateral, superior or inferior SACP (Figure 4A–C, **Left panels)**. Redundant intranodal pacemakers and up to 5 SACPs function as fail-safe mechanisms to ensure robust, uninterrupted SAN pacemaking and conduction even when one or more of them could be dysfunctional due to disease-induced impairments[2]. Due to intramural conduction from SAN-SACP-atria, the surface exits or EASs could be from 5 to 25mm away from the leading intranodal pacemaker. Therefore mapped EASs may be misinterpreted as SAN/atrial pacemaker sites just as with epicardial[16] or endocardial[27] atrial electrogram recordings. In the classic Boineau et al[16] epicardial multi-electrode mapping study, EASs were shown to arise over a region along the CT, which is significantly larger (Figure 5A) than the length of the human anatomical SAN body (~11-29mm). Figure 4A–C (**Middle panels)** show examples of superior/inferior and both multifocal patterns of EASs during sinus rhythm. However, they described a predominant clustering of exit sites along the CT and SVC-RA junction, which correlate well with ex-vivo NIOM human studies[2, 3, 5, 12, 18] (Figures 4 and 5B). Pambrun et al[28] have also reported three main preferential SAN exits using step-wise endocardial high-density 3D catheter mapping in AF patients during stable sinus rhythm (Figure 4A–B, **Right panels**). While currently available data from clinical studies suggest 2-4[28–30] and ex-vivo 3D imaging studies have identified the existence of up to 5 functional SACPs, future studies should investigate if more SACPs exist in human hearts.

Importantly, the SAN leading pacemaker location does not always correlate with the closest SACP[2]. SAN activation can exit via the superior SACPs even though the leading pacemaker could be located in the tail and vice versa (Figure 4A–B, **Left panels**). EASs or SAN exit via the inferior SACP toward the IVC could be misidentified as a second “inferior SAN”.

The SAN is highly innervated compared to surrounding atria and the relative density of innervation is greater in the SAN central region of the SAN than in the tail[31]. Sympathetic activation is known to accelerate SAN pacemakers and shifts EAS to superior SACP and parasympathetic activation can slow sinus rhythm and shift EAS inferiorly but may not correlate with the direction of intranodal pacemaker shift from center to head or tail[22, 32]. The presence of several functional SACPs can lead to beat-to-beat variations in atrial activation[2] and suggest that multifocal atrial activation patterns may correspond to exits from one leading SAN pacemaker through two or more SACPs rather than two anatomically separate, simultaneous leading pacemakers (Figure 4C, **Left panels**).

Recent clinical simultaneous epicardial and endocardial multi-electrode mapping studies of patients with cardiac diseases and AF from de Groot[33] and Kalman[34] groups have also suggested that earliest surface epicardial and endocardial atrial activations during SR may not represent true intramural SAN activation but rather several discrete SAN exits through SACPs. Furthermore, both clinical[27, 29] and ex-vivo NIOM[2] studies show that in diseased hearts the number of functional SACPs/SAN exits can decrease leading to diminished

Author Manuscript Author Manuscript Author Manuscript Author Manuscript

robustness/reserve of the SAN and tachy-brady arrhythmias. SAN impairments due to cardiac diseases can result in decreased number of functional SACPs/SAN exits compared to non-diseased patients[29, 30]. Open-chest endo-epicardial mapping in AF patients showed preferential inferior EASs/SAN exits compared to non-AF patients[33], however, the specific mechanisms causing this phenomenon are not yet completely understood.

TRANSMURAL CONDUCTION IN CT AND SAN EXITS ON EPICARDIAL AND ENDOCARDIAL SURFACES

The CT, often regarded as an arrhythmogenic substrate for micro or macro-reentrant arrhythmia, is identified as a thick muscular ridge (~40-55mm in length and >7mm thick) starting near the junction of the atrial septum and right atrial appendage and ending in the vicinity of the IVC orifice[10]. The location and structure of the CT and close proximity of the SAN are important factors that can lead to the development of SANRT. The CT is highly anisotropic with poor transverse cell-to-cell coupling[35], which could promote both atrial macro-reentry and micro-reentry[36] secondary to slow transversal conduction. Kalman et al[37] found that approximately two thirds of focal right atrial tachycardias were located along the CT and referred to them as “Cristal” Tachycardias. Morris et al’s[38] review of studies where CT tachycardias were successfully ablated in 125 patients, showed that their common origin is in the superior and mid-CT, which overlap with main SAN exits/EAS regions (Figure 5C). As most of the superior, mid-lateral and inferior SAN exits are often observed on the CT in ex-vivo human atria[39], one has to wonder whether majority of focal atrial CT tachycardias, which can be terminated by adenosine[40], involve SAN reentry[37]. Moreover, human NIOM studies of AF mechanisms also suggest that the superior CT-lateral RA is one of the most common sites for reentrant drivers in persistent AF[39], ablation of which is very challenging due to complex 3D architecture of the SVC-superior CT-pectinate muscle junctions with largest wall thickness gradient (1-10mm). For the same reasons, endocardial-only SAN ablation/modification can be technically challenging and is often unsuccessful either due to inadequate transmural lesions to affect intramural SAN pacemakers within the >10mm thickness of the superior CT or the limitations due to the proximity of the phrenic nerve[41].

Sanders et al[42] have shown that SAN modification with radiofrequency ablation at the EAS near the SVC-RA junction may be an effective and safe option for treating SANRT. However, current clinical electroanatomic mapping may not be capable of diagnosing the experimentally reported 1-3mm intranodal microreentries[43], or be able to accurately distinguish whether tachycardia (reentry or enhanced automaticity) originates from SAN pacemakers or from surrounding atrial sources (e.g. SVC or CT). Hence, the heterogeneous results that have been reported for catheter ablation of SAN arrhythmias guided by endocardial mapping[41] are not surprising. Surface mapping may lead to targeting EASs rather than the intramural leading SAN pacemaker, which could be more than 20mm away.

Furthermore, ex-vivo NIOM studies suggest that transmural conduction from intramural SAN pacemaker through superior and/or inferior SACP to atria can lead to differences between epicardial vs endocardial layers where exits from SAN head could be predicted to be seen earlier on epicardium vs endocardium while exits from SAN tail will be

Author Manuscript Author Manuscript Author Manuscript Author Manuscript

seen earlier on endocardium vs epicardium[20, 21](Figure 5D). Parameswaran et al[44] using simultaneous endocardial and epicardial mapping of the human SAN, demonstrated post-pacing caudal shift in SAN exits with marked asymmetry in endo–epicardial exit sites, resulting in significant post-pacing endo–epicardial dissociation of activation (Figure 5E). These findings of complex intramural SAN activation and exit patterns add to the challenges of meaningful electrode mapping.

SAN ARRHYTHMIAS

SANRT usually presents as paroxysms of apparent sinus tachycardia (100-150 beats/min) with abrupt onset and termination[45]. However due to the similarities in P wave morphology and the atrial activation sequence, SAN reentrant arrhythmias can be mistaken for enhanced SAN automaticity. Studies have reported reentrant tachyarrhythmia involving the SAN and surrounding atrial tissue in 2-17% of patients with supraventricular tachycardia[26, 46]. The electrocardiographic similarity of atrial activation during the SAN reentries and normal SR is due to the reentrant excitation exiting the SAN through the preferential SACP, just as in normal SR. Depending on the excitable state of intranodal pacemaker compartments and SACPs, both SAN micro- and macro-reentry involving SACPs can be observed by NIOM in ex-vivo hearts[2, 3, 20](Figure 6). Specifically, these studies revealed intranodal unidirectional block due to heterogeneous refractoriness of SAN pacemaker compartments, which can be enhanced by autonomic modulation with isoproterenol and/or adenosine/acetylcholine and sodium channel blockade[3], as well as extensive interstitial fibrotic strands[2, 20], critical for maintenance of both SAN micro-reentry and macro-reentry. In SAN micro-reentry, pivot waves, anchored to the longitudinal intranodal conduction block, can produce not only tachycardia but even paradoxical bradycardia due to exit block (Figure 6B). In SAN macro-reentry (Figure 6C), a slower SAN wavefront exiting through one SACP (exit) could be followed by excitation of the atria and entering back to SAN via another SACP (entrance), thus forming a reentry circuit with a slow intranodal path and a fast atrial path[2, 3]. The entire SAN macro-reentry cycle length could range ~330-600ms (~100-180bpm), which agrees with clinical studies of SANRT with rates ~110-200 beats/min[45]. Notably, Yamabe et al[26] demonstrated the high efficiency and safety of targeted ablation of the entrance SACP for successful SANRT treatment in all 15 patients studied.

Unlike paroxysmal SANRT, it remains unclear if a definitive reentrant mechanism can drive other forms of SAN arrhythmias including inappropriate sinus tachycardia (IST)[47], a persistent tachycardia characterized by heart rates >100 beats/min. IST causal mechanisms are unknown[45, 48], which limits targeted treatments. Ivabradine, an effective blocker of I_f is prescribed for IST, but its potential for teratogenic effects limits pharmacological treatment options for IST patients that are primarily young females of childbearing age[49]. Catheter ablations aim at “SAN ablation” or “SAN modification” to treat IST by reducing heart rate >50% from the baseline or a minimum of 25% reduction under catecholamine infusion respectively. Rodríguez-Mañero et al[41] in their retrospective review of IST catheter ablation found 86.4% survival free from symptoms but associated with a 50% pacemaker implantation rate.

Author Manuscript Author Manuscript Author Manuscript Author Manuscript

Recently, IST has often been reported in patients with post-COVID-19 syndrome. Aranyo et al[50] found post-COVID-19 IST accompanied by a decrease in heart rate variability related to cardiovagal tone, which suggest imbalances in the autonomic nervous system leading to decreased parasympathetic activity as a causal mechanism. SAN arrhythmias can be secondary to dysautonomia or impairments of the autonomic system that can accelerate or suppress SAN automaticity[51, 52]. Future studies should determine if autonomic imbalances can cause IST and how best to discern this cause, which can lead to improved and targeted treatment options.

ADENOSINE CAN DIFFERENTIATE SAN ARRHYTHMIA MECHANISMS

Adenosine, an endogenous metabolite of the heart, activates adenosine A1 cardiac receptors and G-protein coupled GIRK1-4 channels mediated potassium current $I_{KAdo/ACh}$, which has been suggested to be primarily responsible for SAN cell hyperpolarization and pacemaking slowing in rabbit[53] and canine SAN[20, 54]. In particular, ex-vivo human SAN studies revealed that activation of $I_{KAdo/ACh}$ current by adenosine-induced bradycardia and long atrial pauses due to inhibition of both SAN intranodal pacemaking and slow I_{CaL}-dependent conduction as well as exit blocks in SACPs[2, 3]. Earlier clinical studies showed that an intravenous adenosine bolus can effectively differentiate between atrial and SAN arrhythmias[40]. Adenosine bolus effectively terminates SANRT[55], primarily due to inhibition of I_{CaL}-dependent SAN pacemaker cell excitability and slow conduction similar to atrioventricular node reentrant tachycardia. In a recent study Yamabe et al[26] showed that adenosine bolus and vagal maneuvers terminated SANRT in all 15 patients. As discussed above, we also suggest that as focal CT tachycardias are often adenosine-sensitive[40] one must consider the high likelihood of they being SAN reentry and ablation at the entrance SACP may represent a more effective target than SAN exits on a thick anisotropic CT (Figure 6C).

Unlike SANRT, Still et al[56], reported that in 18 IST patients, adenosine only slightly slowed heart rate compared to patients with normal SR and suggested that the negative chronotropic response to adenosine could be impaired in IST patients. Inefficacy of adenosine in terminating IST also suggests that intranodal SAN reentries may not be a cause of IST or the source can be outside the SAN (e.g., CT). Adenosine testing could potentially confirm IST diagnosis and discriminate other possibilities.

APPROACHES FOR OPTIMAL TRANSMURAL ABLATION OF SAN AND CT ARRHYTHMIAS

Clinically, SAN functional location is often based on the EAS near the SVC base to avoid targeting the SAN. This location is the SAN exit via the superior SACP and not the leading SAN pacemaker located within the intramural SAN structure, which may negatively impact the ablation procedure outcome (Figure 7A). SAN pacemaker and CT structures can be visualized by high resolution delayed-enhancement MRI (DE-MRI) imaging in human hearts[12] (Figure 7B), to avoid the thickest portions (~7-14mm) of the CT when placing endocardial lesions for optimal transmural delivery. Intra-cardiac echocardiography can guide accurate placement of the catheter along the CT to precisely

Author Manuscript Author Manuscript Author Manuscript Author Manuscript

target vulnerable intramural arrhythmogenic substrates[37,39,57,4]. Furthermore, multidetector computed tomography can help define the septal SACP for targeted ablation of SANRT[58]. Placing an epicardial balloon at the ablation location can protect the phrenic nerve from incidental damage during the procedure[41], which may not be necessary when pulsed-field ablation is commercially available (Figure 7C). SAN electrogram recordings acquired near the anatomical location of the SAN to record the slow and relatively small SAN deflections combined with 3D DE-MRI fibrosis imaging can also help locate the SAN (Figure 7D). High-resolution computed tomography can provide accurate information for locating, measuring thickness of the CT and intramural location of SAN based on the SAN-specific artery[13].

FUTURE DIRECTIONS

Investigating treatment strategies combined with high resolution epicardial and endocardial SAN electrophysiological mapping and 3D structural imaging (e.g. DE-MRI) in large animal models and humans are necessary to differentiate arrhythmia mechanisms and develop safer and efficient patient-specific ablation procedures or pharmacological treatments for SAN arrhythmias. Sex-specific mechanisms of SAN arrhythmias, including adenosine signaling pathways and their interaction with autonomic nerves should be studied in patients and suitable animal models[59].

Acknowledgements:

National Institutes of Health (HL115580, HL135109), Leducq Foundation (TNE FANTASY 19CVD03) and the Bob and Corrine Frick Center for Heart Failure and Arrhythmia, OSU.

REFERENCES

1. Keith A, Flack M. The Form and Nature of the Muscular Connections between the Primary Divisions of the Vertebrate Heart. Journal of anatomy and physiology. 1907;41.
2. Li N, Hansen BJ, Csepe TA, et al. Redundant and diverse intranodal pacemakers and conduction pathways protect the human sinoatrial node from failure. Sci Transl Med. 2017;9:eaam5607. [PubMed: 28747516]
3. Li N, Kalyanasundaram A, Hansen BJ, et al. Impaired neuronal sodium channels cause intranodal conduction failure and reentrant arrhythmias in human sinoatrial node. Nat Commun. 2020;11:512. [PubMed: 31980605]
4. Shimamoto K, Yamagata K, Nakajima K, et al. An anatomical approach to determine the location of the sinoatrial node during catheter ablation. J Cardiovasc Electrophysiol. 2021;32:1320–1327. [PubMed: 33600020]
5. Csepe TA, Zhao J, Hansen BJ, et al. Human sinoatrial node structure: 3D microanatomy of sinoatrial conduction pathways. Progress in Biophysics and Molecular Biology. 2016;120.
6. James TN. Anatomy of the human sinus node. The Anatomical Record. 1961;141.
7. Sánchez-Quintana D, Cabrera JA, Farré J, et al. Sinus node revisited in the era of electroanatomical mapping and catheter ablation. Heart. 2005;91:189–194. [PubMed: 15657230]
8. Shiraishi I, Takamatsu T, Minamikawa T, Onouchi Z, Fujita S. Quantitative histological analysis of the human sinoatrial node during growth and aging. Circulation. 1992;85:2176–2184. [PubMed: 1591834]
9. Chandler N, Aslanidi O, Buckley D, et al. Computer three-dimensional anatomical reconstruction of the human sinus node and a novel paranodal area. Anat Rec (Hoboken). 2011;294:970–979. [PubMed: 21538926]

Author Manuscript Author Manuscript Author Manuscript Author Manuscript

10. Matsuyama TA, Inoue S, Kobayashi Y, et al. Anatomical diversity and age-related histological changes in the human right atrial posterolateral wall. Europace. 2004;6:307–315. [PubMed: 15172655]
11. Kalyanasundaram A, Li N, Gardner ML, et al. Fibroblast-Specific Proteotranscriptomes Reveal Distinct Fibrotic Signatures of Human Sinoatrial Node in Nonfailing and Failing Hearts. Circulation. 2021;144:126–143. [PubMed: 33874740]
12. Csepe TA, Zhao J, Sul LV, et al. Novel application of 3D contrast-enhanced CMR to define fibrotic structure of the human sinoatrial node in vivo. Eur Heart J Cardiovasc Imaging. 2017;18:862–869. [PubMed: 28087602]
13. Saremi F, Krishnan S. Cardiac conduction system: anatomic landmarks relevant to interventional electrophysiologic techniques demonstrated with 64-detector CT. Radiographics. 2007;27:1539–1565; discussion 1566-1537. [PubMed: 18025502]
14. Li N, Csepe TA, Hansen BJ, et al. Molecular Mapping of Sinoatrial Node HCN Channel Expression in the Human Heart. Circ Arrhythm Electrophysiol. 2015;8:1219–1227. [PubMed: 26304511]
15. Boineau JP, Schuessler RB, Hackel DB, et al. Widespread distribution and rate differentiation of the atrial pacemaker complex. Am J Physiol. 1980;239:H406–H415. [PubMed: 6254374]
16. Boineau JP, Canavan TE, Schuessler RB, et al. Demonstration of a widely distributed atrial pacemaker complex in the human heart. Circulation. 1988;77.
17. Bromberg BI, Hand DE, Schuessler RB, Boineau JP. Primary negativity does not predict dominant pacemaker location: implications for sinoatrial conduction. Am J Physiol. 1995;269:H877–H887. [PubMed: 7573531]
18. Fedorov VV, Glukhov AV, Chang R, et al. Optical mapping of the isolated coronary-perfused human sinus node. J Am Coll Cardiol. 2010;56:1386–1394. [PubMed: 20946995]
19. Hansen BJ, Zhao J, Csepe TA, et al. Atrial fibrillation driven by micro-anatomic intramural re-entry revealed by simultaneous sub-epicardial and sub-endocardial optical mapping in explanted human hearts. Eur Heart J. 2015;36:2390–2401. [PubMed: 26059724]
20. Lou Q, Hansen BJ, Fedorenko O, et al. Upregulation of adenosine A1 receptors facilitates sinoatrial node dysfunction in chronic canine heart failure by exacerbating nodal conduction abnormalities revealed by novel dual-sided intramural optical mapping. Circulation. 2014;130:315–324. [PubMed: 24838362]
21. Fedorov VV, Schuessler RB, Hemphill M, et al. Structural and functional evidence for discrete exit pathways that connect the canine sinoatrial node and atria. Circ Res. 2009;104:915–923. [PubMed: 19246679]
22. Fedorov VV, Chang R, Glukhov AV, et al. Complex interactions between the sinoatrial node and atrium during reentrant arrhythmias in the canine heart. Circulation. 2010;122:782–789. [PubMed: 20697021]
23. Anderson RH, Sanchez-Quintana D, Spicer DE, Farre J, Back Sternick E. How does the cardiac impulse pass from the sinus to the atrioventricular node? Heart Rhythm. 2022.
24. Alings AM, Abbas RF, Bouman LN. Age-related changes in structure and relative collagen content of the human and feline sinoatrial node. A comparative study. Eur Heart J. 1995;16:1655–1667. [PubMed: 8881862]
25. Truex RC, Smythe MQ, Taylor MJ. Reconstruction of the human sinoatrial node. Anat Rec. 1967;159:371–378. [PubMed: 5586287]
26. Yamabe H, Orita Y. Demonstration of the Anatomical Tachycardia Circuit in Sinoatrial Node Reentrant Tachycardia: Analysis Using the Entrainment Method. J Am Heart Assoc. 2020;9:e014472. [PubMed: 31928174]
27. Sanders P, Morton JB, Kistler PM, et al. Electrophysiological and electroanatomic characterization of the atria in sinus node disease: evidence of diffuse atrial remodeling. Circulation. 2004;109:1514–1522. [PubMed: 15007004]
28. Pambrun T, Derval N, Duchateau J, et al. Sinus node exit, crista terminalis conduction, interatrial connection, and wavefront collision: Key features of human atrial activation in sinus rhythm. Heart Rhythm. 2022.

Author Manuscript Author Manuscript Author Manuscript Author Manuscript

29. Sanders P, Kistler PM, Morton JB, Spence SJ, Kalman JM. Remodeling of sinus node function in patients with congestive heart failure: reduction in sinus node reserve. Circulation. 2004;110:897–903. [PubMed: 15302799]
30. Stiles MK, Brooks AG, Roberts-Thomson KC, et al. High-Density Mapping of the Sinus Node in Humans: Role of Preferential Pathways and the Effect of Remodeling. J Cardiovasc Electrophysiol. 2010;21:532–539. [PubMed: 19912447]
31. Crick SJ, Wharton J, Sheppard MN, et al. Innervation of the human cardiac conduction system. A quantitative immunohistochemical and histochemical study. Circulation. 1994;89:1697–1708. [PubMed: 7908612]
32. Fedorov VV, Glukhov AV, Chang R. Conduction barriers and pathways of the sinoatrial pacemaker complex: their role in normal rhythm and atrial arrhythmias. Am J Physiol Heart Circ Physiol. 2012;302:H1773–H1783. [PubMed: 22268110]
33. Kharbanda RK, Wesselius FJ, van Schie MS, et al. Endo-Epicardial Mapping of In Vivo Human Sinoatrial Node Activity. JACC Clin Electrophysiol. 2021.
34. Parameswaran R, Kalman JM, Royse A, et al. Endocardial-Epicardial Phase Mapping of Prolonged Persistent Atrial Fibrillation Recordings. Circulation: Arrhythmia and Electrophysiology. 2020;13.
35. Morita N, Kobayashi Y, Horie T, et al. The undetermined geometrical factors contributing to the transverse conduction block of the crista terminalis. Pacing Clin Electrophysiol. 2009;32:868–878. [PubMed: 19572862]
36. Spach MS, Dolber PC, Heidlage JF. Influence of the passive anisotropic properties on directional differences in propagation following modification of the sodium conductance in human atrial muscle. A model of reentry based on anisotropic discontinuous propagation. Circ Res. 1988;62:811–832. [PubMed: 2450697]
37. Kalman JM, Olgin JE, Karch MR, et al. “Cristal tachycardias”: origin of right atrial tachycardias from the crista terminalis identified by intracardiac echocardiography. J Am Coll Cardiol. 1998;31:451–459. [PubMed: 9462592]
38. Morris GM, Segan L, Wong G, et al. Atrial Tachycardia Arising From the Crista Terminalis, Detailed Electrophysiological Features and Long-Term Ablation Outcomes. JACC Clin Electrophysiol. 2019;5:448–458. [PubMed: 31000098]
39. Hansen BJ, Zhao J, Helfrich KM, et al. Unmasking Arrhythmogenic Hubs of Reentry Driving Persistent Atrial Fibrillation for Patient-Specific Treatment. J Am Heart Assoc. 2020;9:e017789. [PubMed: 33006292]
40. Markowitz SM, Nemirovksy D, Stein KM, et al. Adenosine-insensitive focal atrial tachycardia: evidence for de novo micro-re-entry in the human atrium. J Am Coll Cardiol. 2007;49:1324–1333. [PubMed: 17394965]
41. Rodriguez-Manero M, Kreidieh B, Al Rifai M, et al. Ablation of Inappropriate Sinus Tachycardia: A Systematic Review of the Literature. JACC Clin Electrophysiol. 2017;3:253–265. [PubMed: 29759520]
42. Sanders WE Jr., Sorrentino RA, Greenfield RA, et al. Catheter ablation of sinoatrial node reentrant tachycardia. J Am Coll Cardiol. 1994;23:926–934. [PubMed: 8106698]
43. Glukhov AV, Hage LT, Hansen BJ, et al. Sinoatrial node reentry in a canine chronic left ventricular infarct model: role of intranodal fibrosis and heterogeneity of refractoriness. Circ Arrhythm Electrophysiol. 2013;6:984–994. [PubMed: 23960214]
44. Parameswaran R, Lee G, Morris GM, et al. Simultaneous epicardial-endocardial mapping of the sinus node in humans with structural heart disease: Impact of overdrive suppression on sinoatrial exits. Heart Rhythm. 2020;17:2154–2163. [PubMed: 32622994]
45. Cossu SF, Steinberg JS. Supraventricular tachyarrhythmias involving the sinus node: Clinical and electrophysiologic characteristics. Progress in Cardiovascular Diseases. 1998;41.
46. Gomes JA, Hariman RJ, Kang PS, Chowdry IH. Sustained symptomatic sinus node reentrant tachycardia: Incidence, clinical significance, electrophysiologic observations and the effects of antiarrhythmic agents. Journal of the American College of Cardiology. 1985;5.
47. Callans DJ, Schwartzman D, Gottlieb CD, Marchlinski FE. Insights into the electrophysiology of atrial arrhythmias gained by the catheter ablation experience: “learning while burning, Part II”. J Cardiovasc Electrophysiol. 1995;6:229–243. [PubMed: 7620647]

Author Manuscript Author Manuscript Author Manuscript Author Manuscript

48. Olshansky B, Sullivan RM. Inappropriate sinus tachycardia. Europace. 2019;21:194–207. [PubMed: 29931244]
49. Mathew ST, Po SS, Thadani U. Inappropriate sinus tachycardia-symptom and heart rate reduction with ivabradine: A pooled analysis of prospective studies. Heart Rhythm. 2018;15:240–247. [PubMed: 29017929]
50. Aranyo J, Bazan V, Llados G, et al. Inappropriate sinus tachycardia in post-COVID-19 syndrome. Sci Rep. 2022;12:298. [PubMed: 34996973]
51. Debruyne P, Rossenbacker T, Collienne C, et al. Unifocal Right-Sided Ablation Treatment for Neurally Mediated Syncope and Functional Sinus Node Dysfunction Under Computed Tomographic Guidance. Circ Arrhythm Electrophysiol. 2018;11:e006604. [PubMed: 30354289]
52. Bauernfeind RA, Amat YLF, Dhingra RC, et al. Chronic nonparoxysmal sinus tachycardia in otherwise healthy persons. Ann Intern Med. 1979;91:702–710. [PubMed: 496102]
53. Belardinelli L, Giles WR, West A. Ionic mechanisms of adenosine actions in pacemaker cells from rabbit heart. J Physiol. 1988;405:615–633. [PubMed: 2855644]
54. Long VP 3rd, Bonilla IM, Baine S, et al. Chronic heart failure increases negative chronotropic effects of adenosine in canine sinoatrial cells via A1R stimulation and GIRK-mediated IKado. Life Sci. 2020;240:117068. [PubMed: 31751583]
55. Engelstein ED, Lippman N, Stein KM, Lerman BB. Mechanism-specific effects of adenosine on atrial tachycardia. Circulation. 1994;89.
56. Still AM, Huikuri HV, Airaksinen KEJ, et al. Impaired negative chronotropic response to adenosine in patients with inappropriate sinus tachycardia. Journal of Cardiovascular Electrophysiology. 2002;13. [PubMed: 11843477]
57. Kalman JM, Lee RJ, Fisher WG, et al. Radiofrequency catheter modification of sinus pacemaker function guided by intracardiac echocardiography. Circulation. 1995;92:3070–3081. [PubMed: 7586278]
58. Sanchez-Quintana D, Anderson RH, Cabrera JA, et al. The terminal crest: morphological features relevant to electrophysiology. Heart. 2002;88:406–411. [PubMed: 12231604]
59. Scherlag BJ, Yamanashi WS, Amin R, Lazzara R, Jackman WM. Experimental Model of Inappropriate Sinus Tachycardia: Initiation and Ablation. Journal of Interventional Cardiac Electrophysiology. 2005;13:21–29. [PubMed: 15976974]
60. Kalyanasundaram A, Li N, Fedorov VV. Mechanisms of normal and dysfunctional sinoatrial nodal excitability and propagation Zipes and Jalife's Cardiac Electrophysiology:From cell to bedside. 8 ed.: Elsevier; 2021: 316–329.

Author Manuscript Author Manuscript Author Manuscript Author Manuscript

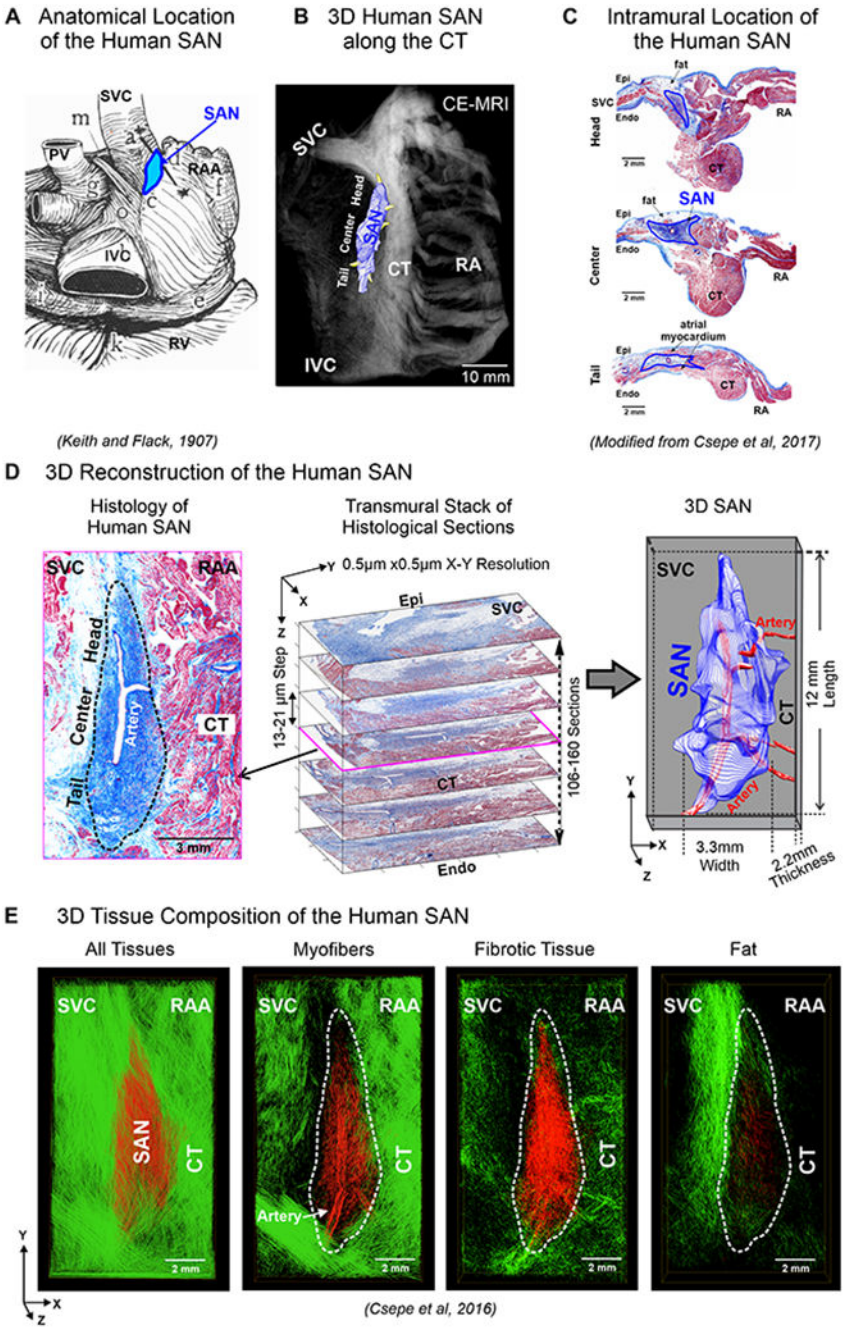

Figure 1:

A. Anatomical location of human SAN. B. 3D SAN structure superimposed on CE-MRI, located along the crista terminalis (CT). C. Histology section with Masson's trichrome staining shows the intramural location of the human SAN. D. Left, Masson's trichrome staining shows human SAN fibrosis (blue). Middle, serial histology of SAN sections representing the transmural thickness of the SAN, stacked to generate computational 3D human SAN (Right). E. 3D computational structural analysis by fiber tracking approach

displays microstructure of myofibers, fibrotic tissue, and fat in the human SAN complex (red) and surrounding atrial tissue (green). (Modified from[1,12,5]).

Author Manuscript Author Manuscript Author Manuscript Author Manuscript

Author Manuscript Author Manuscript Author Manuscript Author Manuscript

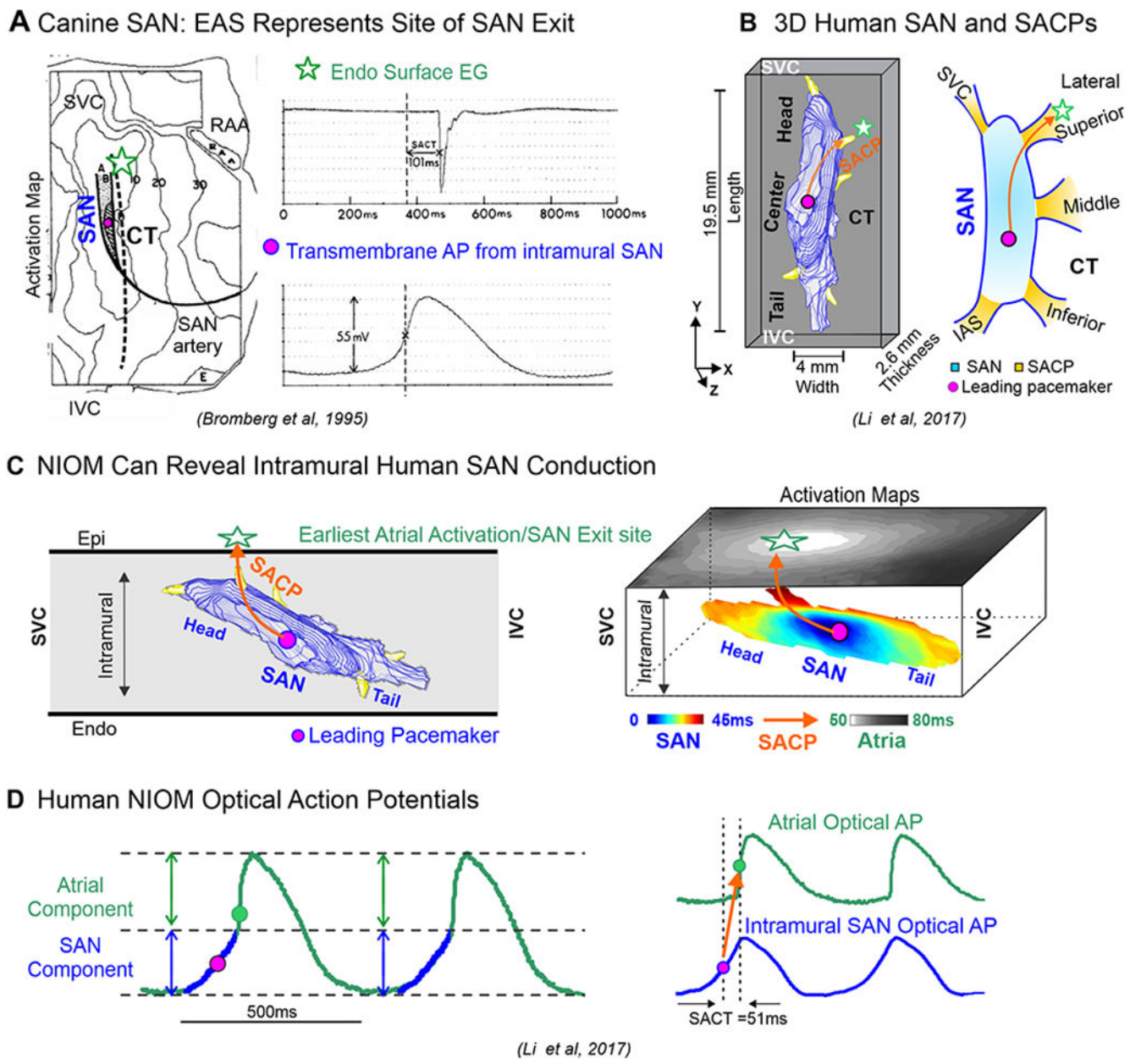

Figure 2:

A. Microelectrode recording and surface unipolar multi-electrode mapping of the canine SAN preparation shows that earliest atrial activation (star) occurred more than 100 ms later and 10 mm away from the SAN leading pacemaker. B. 3D human SAN model with SACPs. C. Schematic to show intramural location of the human SAN, and Near-infrared optical mapping (NIOM) SAN and atrial activation maps showing intramural SAN conduction. D. Left, Human SAN and atrial optical action potentials (OAPs) recorded from ex-vivo NIOM experiments. (Modified from[17,2]).

Author Manuscript Author Manuscript Author Manuscript Author Manuscript

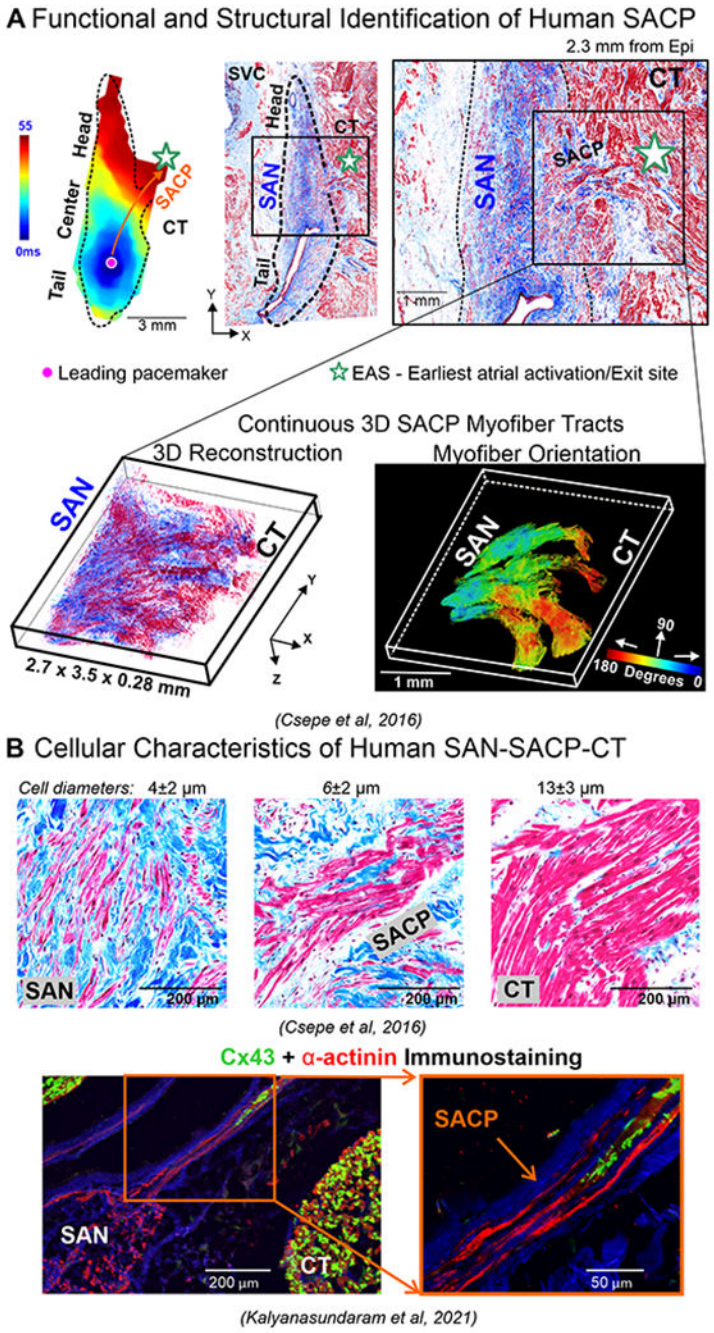

Figure 3.

A. Top left, schematic of human SAN showing SACPs; Middle, near-infrared optical mapping revealed conduction within the SAN complex; Right, histology section of the same lateral region shows the SACP region. Bottom, 3D reconstruction of serial histological sections and computational myofiber tracking of the SACP region containing continuous myofiber tracts between the SAN and atria. B. Top panels, high resolution histological images. Bottom panels, immunostaining images of Cx43 and α-actinin in SACPs. (Modified from[2,5,60]).

Author Manuscript Author Manuscript Author Manuscript Author Manuscript

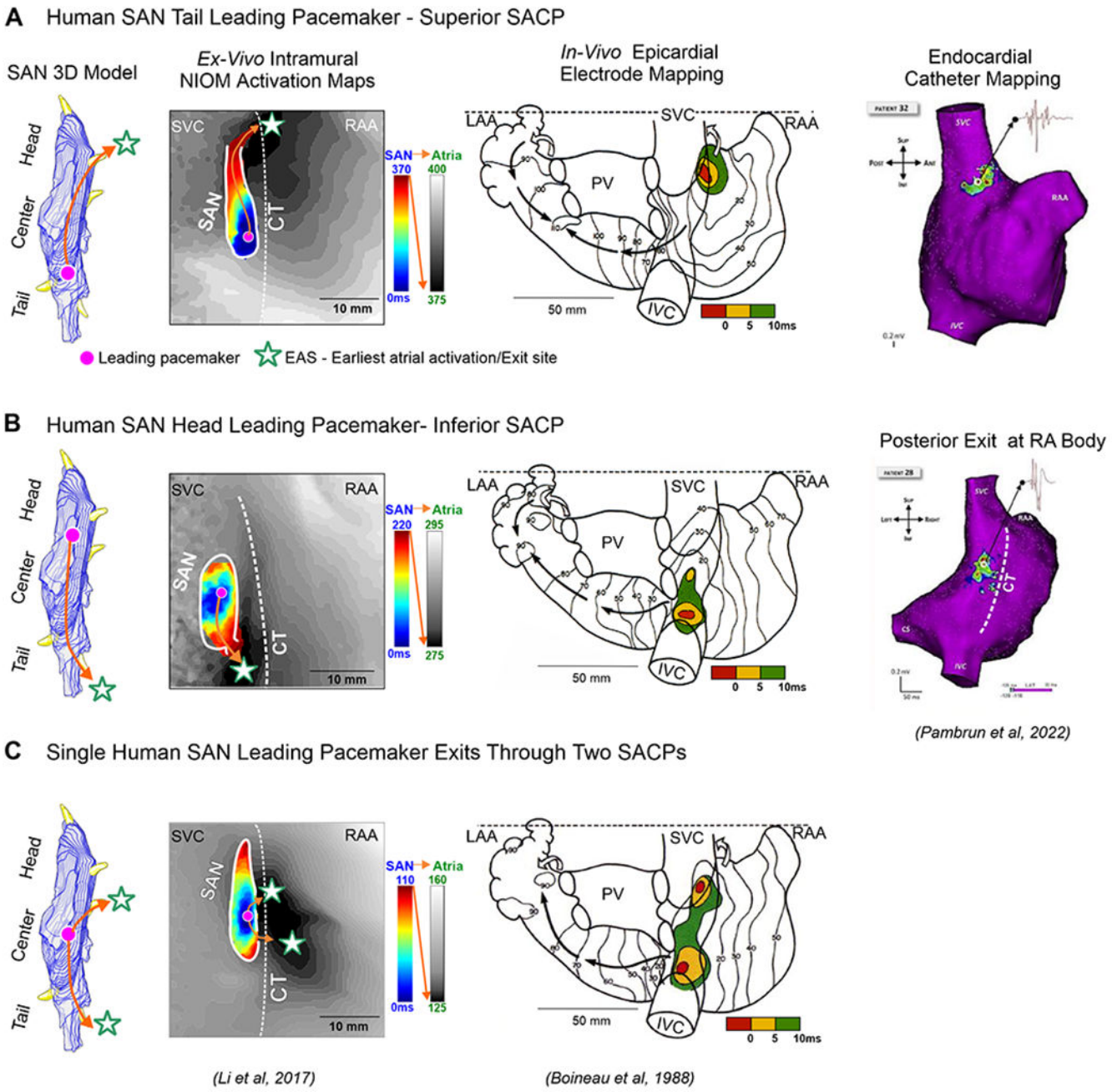

Figure 4:

Human SAN 3D model showing activation exits either via superior/inferior or both SAN conduction pathways. A-C, Left panels: The ex-vivo human SAN NIOM studies show SAN activation exiting either through superior/inferior or both SACPs rather than two different leading pacemakers. A-C, Middle panels: Human epicardial multi-electrode mapping studies show three examples of superior, inferior and both superior and inferior patterns of earliest atrial activation during sinus rhythm (SR). A-B, Right panels: Two main preferential SAN exits demonstrated with step-wise endocardial high-density catheter mapping in AF patients during stable SR. (Modified from[2, 16,28]).

Author Manuscript
Author Manuscript
Author Manuscript
Author Manuscript

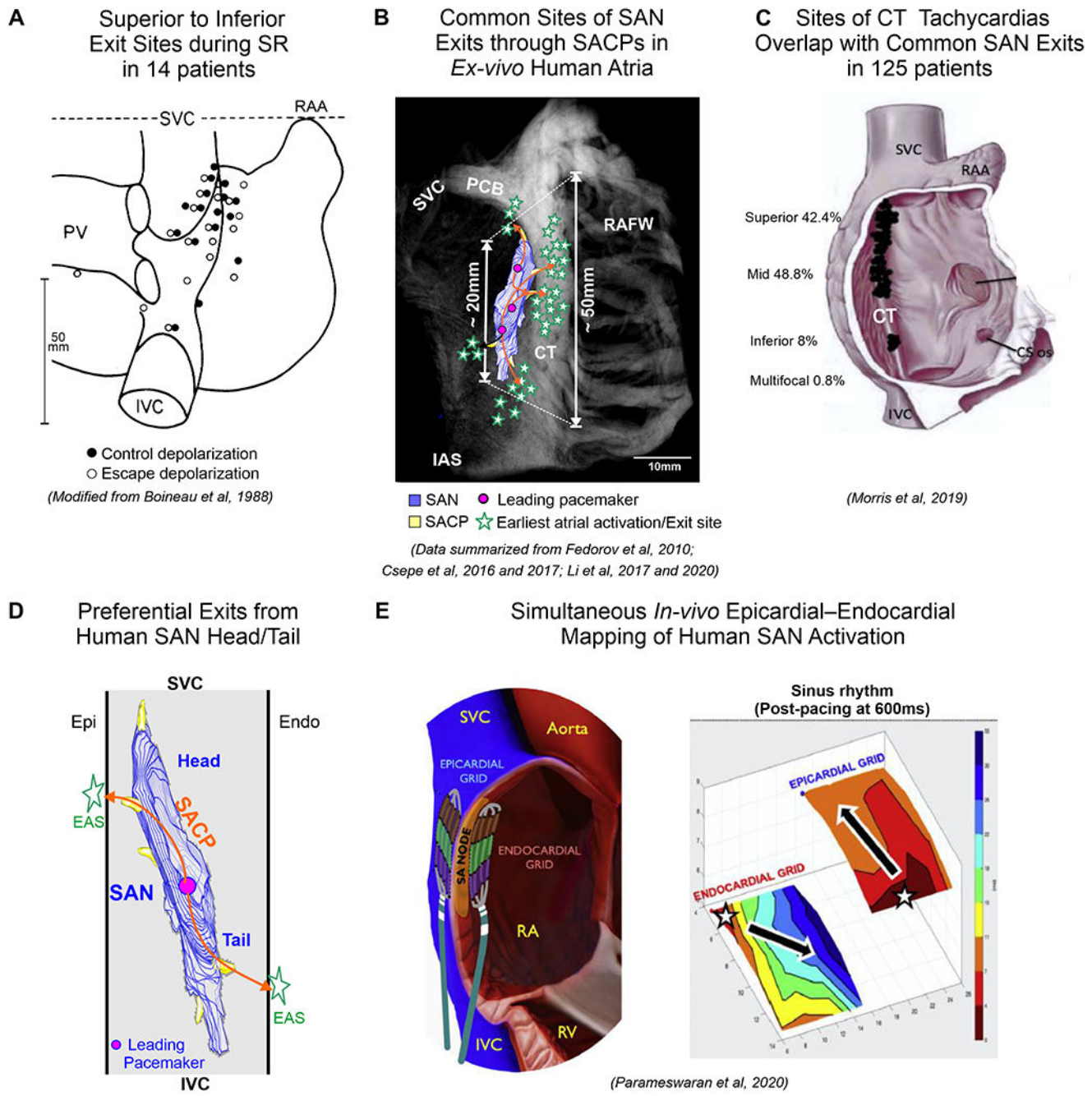

Figure 5:

A: Widespread distribution of the earliest atrial activation sites (EAS) recorded with epicardial bipolar electrodes in patients. The EAS formed a widely distributed region along the CT which greatly exceeded dimensions of the human SAN. B. Ex-vivo CE-CMR with human 3D SAN model showing common EAS/Exit sites from SAN via superior, middle and inferior SACPs defined by NIOM in ex-vivo human studies[18,5,12,2,3]. C. Distribution of successful ablation sites of atrial tachycardias on the CT. 3D SAN model showing surface exit sites via the superior and inferior SACPs near the SAN head and tail, respectively.

Author Manuscript Author Manuscript Author Manuscript Author Manuscript

E. Simultaneous endocardial-epicardial mapping of the SAN /CT showing post-pacing caudal shift in activation exits with marked asymmetry in endo–epi exit sites. (Modified from[16,38,44]).

Author Manuscript Author Manuscript Author Manuscript Author Manuscript

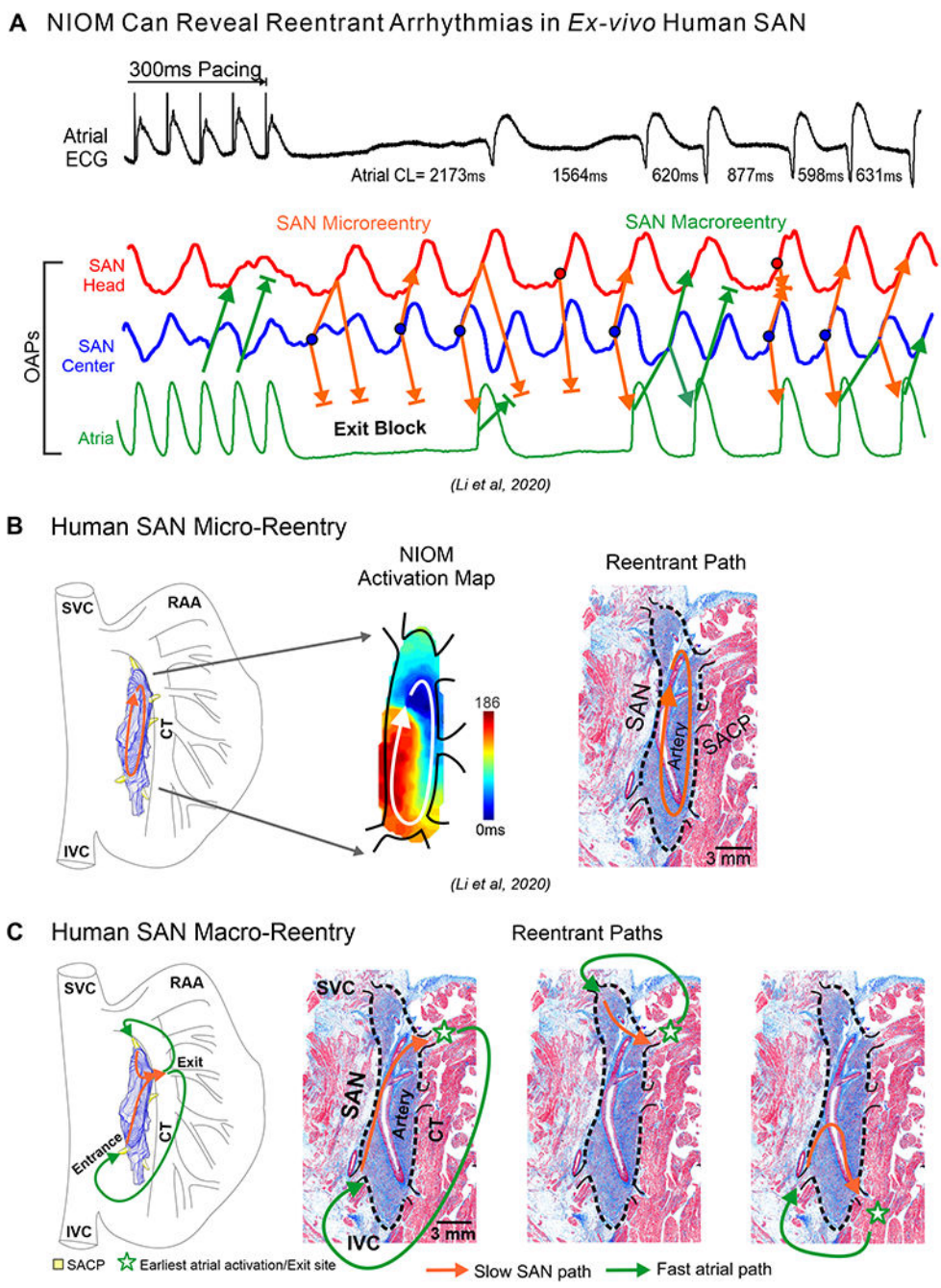

Figure 6:

A. Top to bottom, atrial ECG, SAN and atrial OAPs show pause, exit block, and SAN reentrant arrhythmias after 300ms atrial pacing in the ex-vivo human heart; B. SAN 3D model, activation maps and histology sections of microreentry path; C. Macro-reentrant paths within the SAN-SACP-atria structure. (Modified from[3,2]).

Author Manuscript Author Manuscript Author Manuscript Author Manuscript

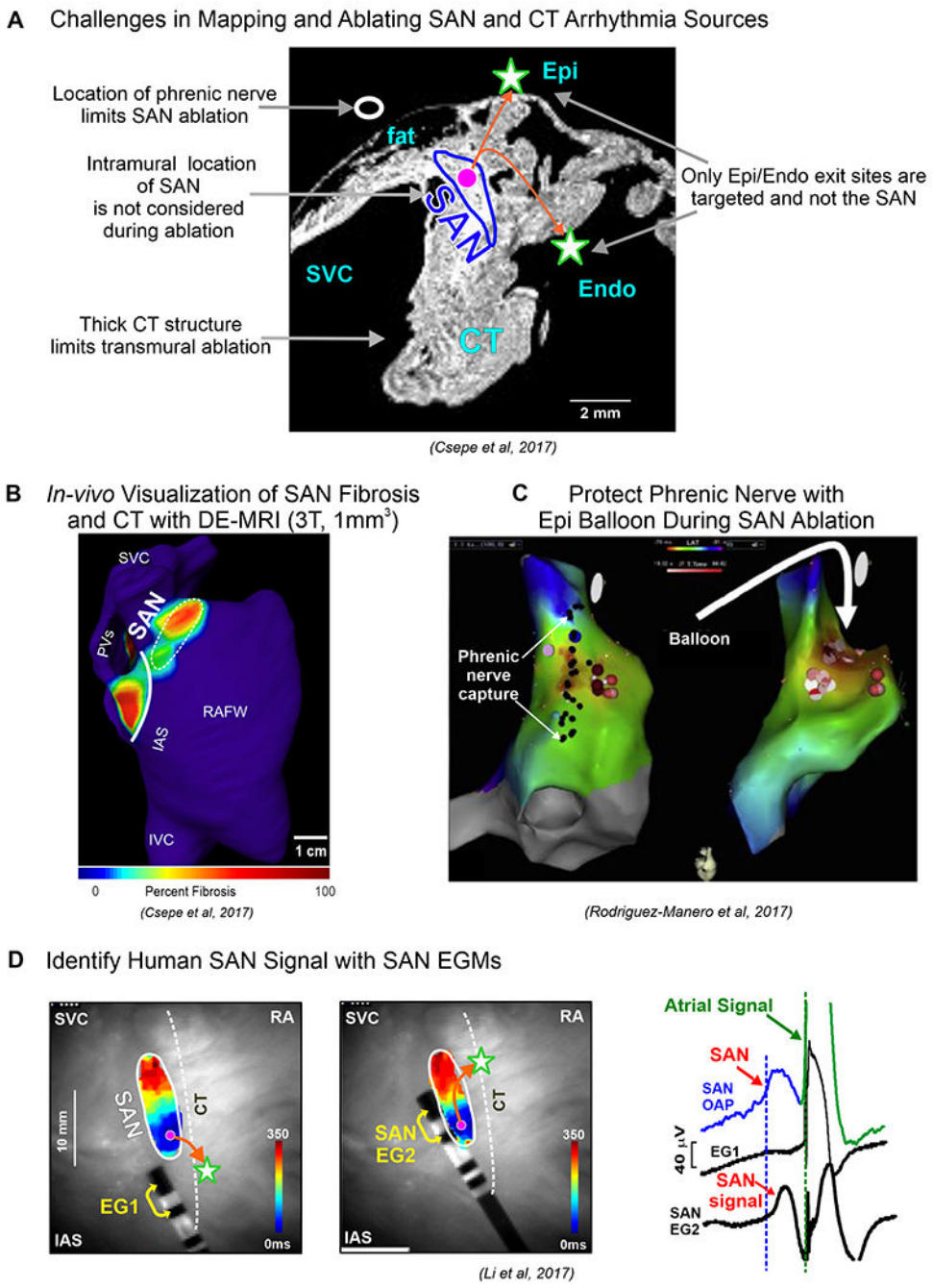

Figure 7:

A. Central panel describes challenges in mapping and ablating human SAN arrhythmias. B. DE-MRI can be utilized to visualize SAN and CT. C. Damage to phrenic nerve can be avoided by utilizing an epicardial balloon. D. SAN can be identified with SAN electrogram (EG) recorded from electrodes placed close to the SAN. (Modified from[12,2,41]).